Relativistic formulation of the Voigt profile

P. Wcisło,[1] P. Amodio,[2] R. Ciuryło,[1] and L. Gianfrani[2]
[1]*Institute of Physics, Faculty of Physics, Astronomy and Informatics, Nicolaus Copernicus University, Grudziadzka 5, 87-100 Torun, Poland*
[2]*Department of Mathematics and Physics, Second University of Naples, Viale Lincoln 5, 81100 Caserta, Italy*
(Received 28 November 2014; published 17 February 2015)

The relativistic formulation of the Voigt profile is reported for the spontaneous emission from an atomic or molecular cloud, in coincidence with a given spectral line. We considered the simultaneous occurrence of homogeneous broadening and thermal broadening, this latter being determined by the relativistic Doppler effect. Our formula for the relativistic Voigt profile reproduces those characterizing the two available limit cases, namely, the relativistic Gaussian profile and the classical Voigt convolution. The relativistic deformation of the Voigt profile was carefully quantified at different temperatures, in the case of the molecular hydrogen spectrum.

DOI: 10.1103/PhysRevA.91.022508 PACS number(s): 32.70.Jz

I. INTRODUCTION

The spectral lines, their shapes and their widths, either in absorption or emission spectroscopy, are powerful tools for gas and plasma diagnostics in a variety of physical systems and environments, including stellar and planetary atmospheres, interstellar gas clouds, exhaust gases from combustion processes, and plasma plumes from laser ablation or flames. These examples are characterized by extreme thermodynamic conditions, in which the temperature can be as high as thousands of kelvin. The standard Voigt profile, which is a convolution of Gaussian and Lorentzian profiles, represents the commonly used line-shape model, simultaneously taking into account Doppler and collisional broadening effects. With the growing precision of laser spectroscopy, one may wonder when the relativistic Doppler effect becomes significant and to what extent it affects the shape of the spectral lines.

High spectral fidelity is a relatively new feature of modern atomic and molecular spectroscopy, implemented in few specialized laboratories and mostly due to the recent availability of optical frequency comb synthesizers [1]. It can be obtained when using a tunable laser with a sufficiently narrow emission, such as an extended cavity diode laser or a quantum cascade laser, to probe the species of interest, in conjunction to the comb, which simply provides a frequency ruler against which the tunable laser can be calibrated [2–5]. If the spectral fidelity is accompanied by a sufficiently high signal-to-noise ratio (SNR), interesting line-shape investigations can be carried out [6], aimed at a better understanding of the physical mechanisms determining the absorption profile associated with a given spectral line. In this respect, exceptionally precise measurements of absorption line shapes have been very recently reported by Cygan *et al.*, on the $^{16}O_2$ B band at 689 nm [7]. It should be mentioned that at some level of accuracy the relativistic effect can be an issue also for the spectroscopic determination of the Boltzmann constant by means of Doppler broadening thermometry [8,9].

Similarly, the relativistic Doppler effect might be considered in astronomical spectroscopy in the near future. In fact, sophisticated astrophysical models require high-quality spectra with increasing resolution and accuracy. This is stimulating the development of high-resolution stellar spectrometers at the largest telescopes [10]. A famous example is given by the Potsdam Echelle Polarimetric and Spectroscopic Instrument (PEPSI) at the Large Binocular Telescope Observatory of Tucson, Arizona, whose installation and testing began in July 2014 [11]. The PEPSI project is designed to provide stellar spectra from 390 and 1050 nm, with a signal-to-noise ratio of 5000 and a resolution (defined as $\lambda/\Delta\lambda$) of 320 000 [12].

In a recent paper, a new formulation of the relativistic Doppler-broadened line profile, based upon the relativistic Doppler effect, has been proposed [13]. This work has demonstrated the failure of the commonly accepted prediction, which was reported in the pioneering work of Gerbal and Prud'Homme[14].

In the present paper, we calculate the relativistic Voigt profile and investigate the difference between the relativistic and the classical Voigt profiles as a function of the gas temperature. Our attention is focused on one of the most promising candidates for the observation of the relativistic corrections to the emissive line profiles, namely, molecular hydrogen [15–18]. As is well known, this species is of great interest in astrophysics [19–22]. In particular, molecular hydrogen is the most abundant molecule in the atmospheres of cool stars and its quadrupole lines in the infrared act as a sensitive probe [23], similar to the atomic hydrogen lines in hot stars [24].

II. EMISSIVE RELATIVISTIC VOIGT PROFILE

In this section we present a derivation of the relativistic Voigt profile. Presently, we are focused only on the spontaneous emission process. Note that the other two process related to the problem of the shape of molecular or atomic transitions, absorption, and stimulated emission, should be considered in a different way.

In the relativistic case, the final result depends on the details of the considered source of light and the detection system. Therefore it is crucial to precisely define the whole physical problem. Let us assume that in the laboratory frame we observe a cloud that contains N_{mol} molecules. In the real physical system the rate of photons emission will depend on the excitation mechanism, whose description is beyond the scope of this paper. We denote the number of photons emitted per second by a single molecule in the molecule and laboratory frames by σ' and σ, respectively. Due to the invariance of the number of photons these two quantities are dependent via the

following relation:

$$\sigma' dt' = \sigma dt, \tag{1}$$

where dt' and dt are time intervals in the molecule (S') and laboratory (S) frames, respectively. In the simplest case, it can be assumed that σ does not depend on molecule velocity. When the rate of excitation events is much smaller than the rate of spontaneous emission then the rate of photons emission will almost not be influenced by the rate of spontaneous emission. In other words, the rate of photon emissions will be determined by the dynamics of excitation processes. Therefore it seems more natural to assume that the rate of photons emission in the laboratory frame σ is the same for all molecules. The same assumption was adopted in Ref. [13]. Note that it follows from Eq. (1) that if σ is speed independent then σ' is speed dependent, because dt/dt' is a function of speed.

Note also that if the opposite assumption was taken, i.e., speed-independent rate of photons emission in the molecule frame, then the transformation of the time will lead to additional speed-dependent factor in the laboratory frame. The consequence of it will be that a normalized profile assumed in the molecule frame will not lead to a normalized profile in the laboratory frame. However, in general, the normalization integral does not have to be Lorentz invariant and the change of the profile normalization under the Lorentz transformation does not imply that the model assumptions are unphysical.

As it is in the case of classical Voigt profile, we assume that in the molecule frame the frequency distribution of photons is given by the Lorentz profile $I_{\mathrm{LP}}(\omega') = (1/\pi)\Gamma'/(\Gamma'^2 + (\omega' - \omega'_0)^2)$, where Γ' is the half width at half maximum and ω' and ω'_0 are the frequency of emitted photon and the transition frequency, respectively. The physical quantities in S' and S are denoted with and without prime, respectively. Note that the choice of the Lorentzian distribution assumes isotropic line-broadening collisions in S'. It should be noted that for simplicity we neglect any speed dependence of Lorentzian width as well as velocity-changing collisions, which can affect the spectral line shape [25].

Let us consider a class of molecules having a momentum $\vec{p}$. In their frame, S', the number of photons emitted by each molecule into the solid angle $d\Omega'$ having frequency ω' is $(\sigma' dt')I_{\mathrm{LP}}(\omega')d\omega' d\Omega'/(4\pi)$. Hence, the total number of photons emitted by the molecules of the momentum class is

$$dN'_{\mathrm{phot}} = \sigma' dt' I_{\mathrm{LP}}(\omega') d\omega' \frac{d\Omega'}{4\pi} N_{\mathrm{mol}} f(\vec{p}) d^3\vec{p}, \tag{2}$$

where $f(\vec{p})$ is the relativistic momentum distribution in the S frame. For simplicity we assume that in S the cloud remains at rest or moves at speed much smaller than the mean speed of its thermal distribution, hence the momentum distribution is not shifted with respect to thermal distribution. Note that this assumption does not influence the derivation of classical Voigt profile.

Following transformation of the time and space coordinates [26] to transform the frequency, the solid angle element, and the time interval from S' to S we used the following relations [27]:

$$\frac{\omega'}{\omega} = \frac{d\omega'}{d\omega} = \frac{dt}{dt'} = \kappa, \quad \frac{d\Omega'}{d\Omega} = \kappa^{-2}, \tag{3}$$

being

$$\kappa = \gamma(1 - \beta\cos\xi), \tag{4}$$

where $\gamma = 1/\sqrt{1-\beta^2}$, $\beta = v/c$, and ξ is an angle, in the S frame, between photon wave vector $\vec{k}$ and molecule velocity $\vec{v}$. The number of photons is invariant, namely, $dN'_{\mathrm{phot}} = dN_{\mathrm{phot}}$, hence the number of photons in S per solid angle element $d\Omega$, per frequency interval $d\omega$, per unit time is

$$\frac{dN_{\mathrm{phot}}}{d\Omega d\omega dt} = \frac{dN'_{\mathrm{phot}}}{d\Omega' d\omega' dt'} \frac{d\Omega' d\omega' dt'}{d\Omega d\omega dt} = \frac{\sigma}{4\pi}\kappa^{-1} I_{\mathrm{LP}}(\kappa\omega) N_{\mathrm{mol}} f(\vec{p}) d^3\vec{p}. \tag{5}$$

In Eq. (5) we used Eq. (1), which states that $\sigma = \sigma' dt'/dt$. In thermodynamic equilibrium, the relativistic momentum distribution $f(\vec{p})$ is proportional to the Boltzmann energy distribution, namely, $f(\vec{p}) \propto e^{-E/k_B T}$, where k_B is the Boltzmann constant, T the gas temperature, $E = m_0c^2\gamma = m_0c^2\sqrt{1 + p^2/(m_0c)^2}$ and $\vec{p} = m_0\gamma\vec{v}$ is momentum of emitter. Taking into account the normalization condition $\int f(\vec{p}) d^3\vec{p} = 1$, the relativistic momentum distribution can be written as

$$f(\vec{p}) = \frac{1}{4\pi\alpha(m_0c)^3 K_2(1/\alpha)} e^{-\gamma/\alpha}, \tag{6}$$

where $\alpha = k_B T/(m_0c^2)$ and $K_N(z)$ is the modified Bessel function of the Nth order. In the spherical coordinates the $d^3\vec{p}$ element can be written as $d\varphi d\theta \sin\theta p^2 dp = (m_0c)^3 d\varphi d\theta \sin\theta\gamma\sqrt{\gamma^2 - 1} d\gamma$ [note that $\gamma = \sqrt{1 + p^2/(m_0c)^2}$], where the angles φ and θ are defined in Fig. 1.

The total number of photons emitted by all momentum classes in the laboratory frame per solid angle element $d\Omega$, per frequency interval $d\omega$, per unit time can be found by integrating Eq. (5) over the whole momentum space

$$I_{\mathrm{RVP}}(\omega) = \frac{\sigma}{(4\pi)^2} \int_1^\infty d\gamma \int_0^\pi d\theta \int_0^{2\pi} d\varphi \sin\theta \kappa^{-1} I_{\mathrm{LP}}(\kappa\omega) \times \left\{ \frac{N_{\mathrm{mol}}}{\alpha K_2(1/\alpha)} e^{-\gamma/\alpha} \gamma\sqrt{\gamma^2 - 1} \right\}. \tag{7}$$

Here, we took advantage from the assumption, discussed in the beginning of this section, that σ does not depend on the velocity. The expression in curly brackets is known as the

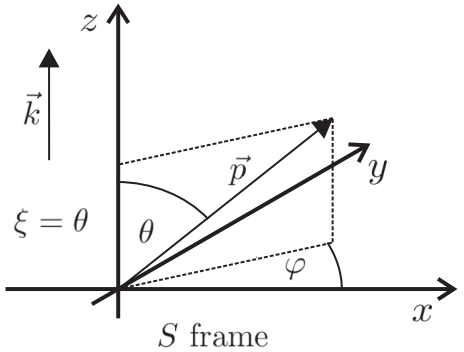

FIG. 1. Angles and vectors in the S frame.

Jüttner distribution [13,28]. The integral over φ is trivial, since no term depends on it. If we assume that the observation direction is parallel to the z axis, see the $\vec{k}$ wave vector in Fig. 1, then $\xi = \theta$ and Eq. (7) can be explicitly written as

$$I_{\mathrm{RVP}}(\omega) = \frac{\sigma}{8\pi^2}\frac{N_{\mathrm{mol}}}{\alpha K_2(1/\alpha)}\int_1^\infty d\gamma e^{-\gamma/\alpha}\sqrt{\gamma^2-1}\int_0^\pi d\theta \sin\theta \times \frac{1}{1-\beta\cos\theta}\frac{\Gamma'}{\Gamma'^2+[\gamma(1-\beta\cos\theta)\omega-\omega_0']^2}. \quad (8)$$

It should be noted that $\beta = \sqrt{\gamma^2-1}/\gamma$. The integral over the θ angle can be carried out analytically, thus leading to our final formula for the relativistic Voigt profile

$$I_{\mathrm{RVP}}(\Delta\omega) = \frac{\sigma_0}{\pi\beta_m K_2(2/\beta_m^2)}\frac{\Gamma'}{\beta_m^2\Gamma'^2+\omega_D^2}\int_1^\infty d\gamma \times e^{-2\gamma/\beta_m^2}\gamma\left\{\frac{\omega_D}{\Gamma'}[\arctan(\xi_+(\gamma))-\arctan(\xi_-(\gamma))] + \beta_m \ln\left(\frac{1+\sqrt{1-\gamma^{-2}}}{1-\sqrt{1-\gamma^{-2}}}\right) + \frac{1}{2}\beta_m \ln\left(\frac{1+\xi_-^2(\gamma)}{1+\xi_+^2(\gamma)}\right)\right\}, \quad (9)$$

where

$$\xi_\pm(\gamma) = \frac{\Delta\omega}{\Gamma'}(\gamma \pm \sqrt{\gamma^2-1}) + \frac{\omega_D}{\Gamma'}\frac{\gamma \pm \sqrt{\gamma^2-1}-1}{\beta_m} \quad (10)$$

and $\sigma_0 = \sigma N_{\mathrm{mol}}/(4\pi)$. To be consistent with a common line-shape notation we introduced in Eqs. (9) and (10) $\omega_D = (v_m/c)\omega_0'$ and $\Delta\omega = \omega - \omega_0'$. Moreover we replaced the α parameter, exploited in Ref. [13], with $\beta_m = v_m/c$, which seems to be more intuitive and easier to interpret ($\alpha = \beta_m^2/2$). By v_m we mean the most probable speed of classical nonrelativistic Boltzmann distribution ($v_m = \sqrt{2k_BT/m_0}$). Note that within this notation the relativistic Voigt profile is described by two parameters characterizing also the classical Voigt profile (ω_D and Γ'), and one extra parameter β_m, which controls how important the relativistic effects are. It should be also noted that in general both the classical and the relativistic Voigt profiles depend on the same set of physical parameters, however the classical Voigt profile effectively depends only on the product of $\sqrt{T}$ and ω_0 ($\omega_D \propto \sqrt{T}\omega_0$), hence mathematically it is defined by one parameter less. This property is also related to the physical interpretation of the relativistic Voigt profile. One needs to remember that keeping constant the ω_D parameter and increasing the β_m parameter physically means that the temperature is increasing, while the line position ω_0' is decreasing such as to keep ω_D unchanged. It should be noted that in the weak relativistic limit (small β_m) a special approach to numerically evaluate the integral from Eq. (9) needs to be applied, see Appendix A.

In the next two sections we show that our formulation of the relativistic Voigt profile is consistent with the formulas for two available limit cases, i.e., classical Voigt profile (Sec. III) and relativistic Doppler profile (Sec. IV). Finally, in Appendix B, we show analytically that the profile given by Eq. (9) is normalized.

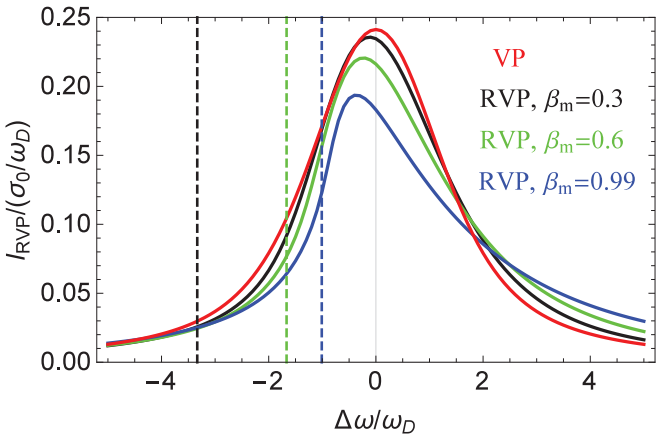

FIG. 2. (Color online) Relativistic Voigt profile for $\Gamma'/\omega_D = 1$. Black, green, and blue lines correspond to $\beta_m = 0.3$, 0.6, and 0.99, respectively. The vertical dashed lines indicate the values of $\Delta\omega$ corresponding to $\omega = 0$. As a reference, also the classical Voigt profile is presented as a red line.

III. CLASSICAL VOIGT PROFILE LIMIT

In this section we show that in the nonrelativistic case, $\beta_m \to 0$, the relativistic Voigt profile given by Eqs. (9) and (10) converges to the common classical formula. Figure 2 presents a comparison between the relativistic and classical Voigt profiles. Note that for highly relativistic cases the broadening is comparable with ω_0' and the left side of the line is cut by the $\omega = 0$ line (see the vertical dashed lines of Fig. 2). In this case, for ω close to zero, the assumption about Lorentzian distribution is not valid any more. It is seen that the asymmetric relativistic profile converges to the classical Voigt profile as β_m goes to zero. This convergence can be easily shown analytically. First, it can be seen that the two logarithmic terms in curly brackets in Eq. (9) are purely relativistic and they disappear as $\beta_m \to 0$. Also the term $\beta_m^2\Gamma'^2$ in the denominator before the integral straightforwardly goes zero. The integral variable γ should be replaced with $x = \sqrt{2(\gamma-1)}/\beta_m$. Then $\xi_\pm \to (\Delta\omega \pm x\omega_D)/\Gamma'$ as β_m goes to zero. Moreover in this limit the modified Bessel function of the second kind can be written as $K_2(2/\beta_m^2) \approx \sqrt{\pi}(\beta_m/2)\exp(-2/\beta_m^2)$. Finally the whole Eq. (9) together with Eq. (10) can be rewritten as

$$I_{\mathrm{RVP}}(\Delta\omega) \xrightarrow{\beta_m\to 0} \frac{2\sigma_0}{\pi^{3/2}\omega_D}\int_0^\infty dx e^{-x^2}x \times\left[\arctan\left(\frac{\Delta\omega + x\omega_D}{\Gamma'}\right) - \arctan\left(\frac{\Delta\omega - x\omega_D}{\Gamma'}\right)\right]. \quad (11)$$

Equation (11) is equivalent to the formula defining the common Voigt profile, for instance see Eq. (52) in Ref. [25].

IV. RELATIVISTIC GAUSS PROFILE LIMIT

The convergence of the relativistic Voigt profile, Eq. (9), to the relativistic Gauss profile, Eqs. (14) and (22) in Ref. [13], for $\Gamma'/\omega_D \to 0$ is presented in Fig. 3. It can be also shown analytically. In this limit the integral over θ from Eq. (8) can

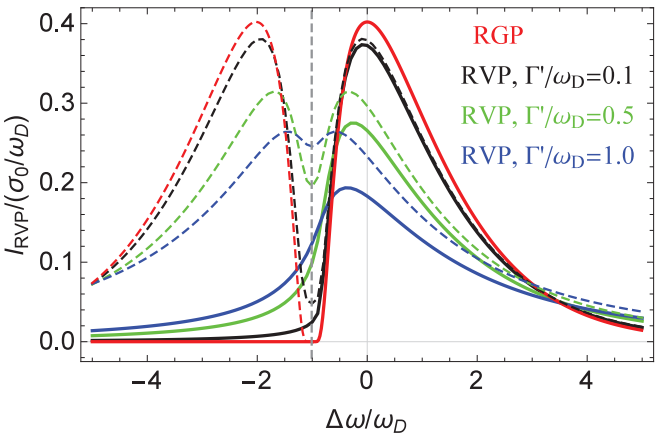

FIG. 3. (Color online) Relativistic Voigt profile for $\beta_m = 0.99$. Black, green, and blue lines correspond to $\Gamma'/\omega_D = 0.1$, 0.5, and 1.0, respectively. The gray vertical dashed line indicates the values of $\Delta\omega$ corresponding to $\omega = 0$. As a reference, also the relativistic Gauss profile is presented as a red line. Thin dashed curves represent the solutions without the rotating wave approximation, see Appendix B.

be written as

$$\int_0^\pi d\theta \sin\theta \frac{1}{1-\beta\cos\theta}\pi\delta[\gamma(1-\beta\cos\theta)\omega-\omega_0'] = \begin{cases} \frac{\pi}{\beta}\frac{1}{\omega_0'} & \text{for} \quad \gamma\omega(1-\beta) < \omega_0' < \gamma\omega(1+\beta), \\ 0 & \text{otherwise,} \end{cases} \tag{12}$$

where $\delta(\cdot)$ is the Dirac δ. Consequently, defining $\gamma_{\min} = \frac{1}{2}(\frac{\omega}{\omega_0'} + \frac{\omega_0'}{\omega})$, the whole Eq. (8) simplifies to

$$\begin{aligned} I_{\mathrm{RVP}}(\omega) &\xrightarrow{\Gamma'\to 0} \frac{\sigma}{8\pi^2}\frac{N_{\mathrm{mol}}}{\alpha K_2(1/\alpha)} \\ &\quad\times \int_{\gamma_{\min}}^{\infty} d\gamma e^{-\gamma/\alpha}\sqrt{\gamma^2-1}\frac{\pi}{\beta}\frac{1}{\omega_0'} \\ &= \sigma_0 \frac{\omega^2+2\alpha\omega_0'\omega+{\omega_0'}^2}{4K_2(1/\alpha)\omega{\omega_0'}^2} e^{-\frac{\omega^2+{\omega_0'}^2}{2\alpha\omega_0'\omega}}. \end{aligned} \tag{13}$$

This result is the same as the emissive relative Doppler profile presented in Ref. [13], see Eq. (22) therein. To compare this profile with other line shapes, as we did before, it is convenient to replace ω_0', ω, and α parameters with ω_D, $\Delta\omega$, and β_m. Then Eq. (13) can written as

$$\begin{aligned} &I_{\mathrm{RVP}}(\omega) \\ &\xrightarrow{\Gamma'\to 0} \sigma_0 \frac{\beta_m^2\Delta\omega^2 + (2+\beta_m^2)\beta_m\omega_D\Delta\omega + (2+\beta_m^2)\omega_D^2}{4K_2(2/\beta_m^2)(\beta_m^{-1}\omega_D+\Delta\omega)\omega_D^2} \\ &\quad\times e^{-\frac{\beta_m^2\Delta\omega^2+2\beta_m\omega_D\Delta\omega+2\omega_D^2}{\beta_m^2\omega_D(\beta_m\Delta\omega+\omega_D)}}. \end{aligned} \tag{14}$$

From this notation of relativistic Doppler profile it is straightforwardly seen that in classical nonrelativistic limit ($\beta_m \to 0$) it converges to the common Gauss profile $I_{\mathrm{GP}} = \sigma_0/(\sqrt{\pi}\omega_D)\exp(-\Delta\omega^2/\omega_D^2)$.

V. ENTITY OF RELATIVISTIC EFFECTS

Molecular hydrogen will be our physical target. Since $\beta_m = v_m/c = \sqrt{2k_BT/(mc^2)}$, atomic and molecular hydrogen are fairly good choices if one wants to look at relativistic effects, because of their small mass. Nevertheless, also other molecules such as O_2 or CO, for which the relativistic deformation is only four times smaller, can be considered as candidates for searching the relativistic effects manifestation. For the case of molecular hydrogen, temperatures between $T = 300$ K and 3000 K correspond to $\beta_m \approx 0.5\times10^{-5}$ and 1.7×10^{-5}, respectively. In Figs. 4(a) and 4(b) we present the differences between relativistic Voigt profiles (RVP) and classical Voigt profiles (VP) for $\beta_m = 10^{-4}$ and 10^{-6}, respectively, for $\Gamma/\omega_D = 1$. For a very wide range of values of the β_m parameter, from 10^{-2} down to 0, the shape of the difference of these two profiles is almost the same, while its amplitude varies with β_m, see Fig. 4(c). The dependence from this figure determines, for a given temperature, the lowest level of signal-to-noise ratio (SNR) of measured spectrum, which is required to distinguish the relativistic deformation of the

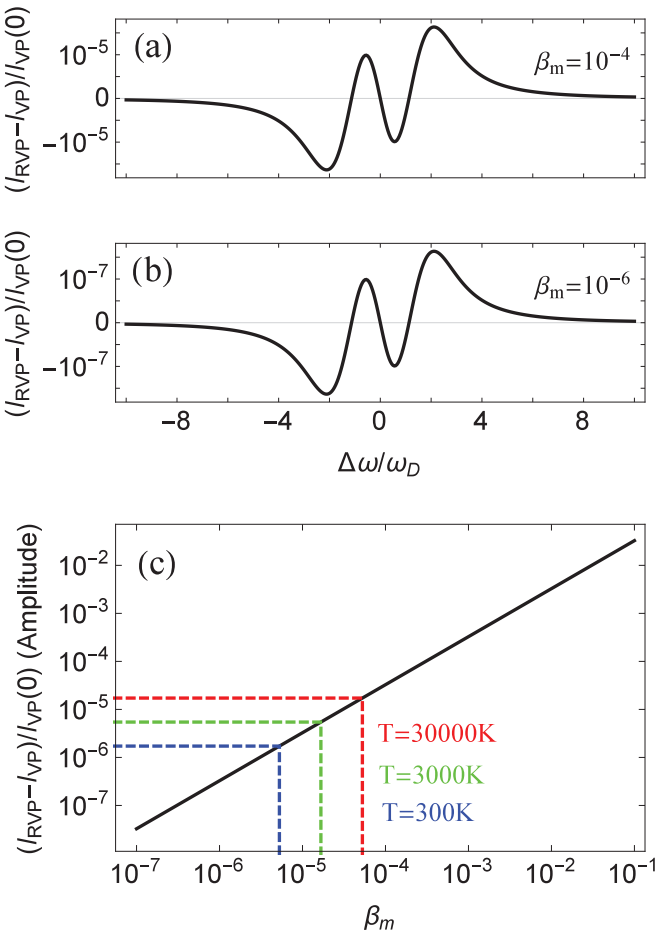

FIG. 4. (Color online) (a) and (b) Differences between RVP and VP normalized to the VP amplitude for $\beta_m = 10^{-4}$ and for $\beta_m = 10^{-6}$, respectively, for $\Gamma/\omega_D = 1$. (c) Amplitude of differences between RVP and VP normalized to the VP amplitude as a function of the β_m parameter. The temperatures denoted in (c) correspond to the selected β_m values. They were calculated in the case of the H_2 molecular mass.

spectra. For the case of molecular hydrogen these levels are $\approx 1/(1.7\times10^{-6}) \approx 5.8\times10^{5}$ and $\approx 1/(3.6\times10^{-6}) \approx 2.8\times10^{5}$ for $T = 300$ K and 3000 K, respectively. In astrophysical conditions, the atomic hydrogen lines in hot stars (at $T \approx 60\,000$ K) [24] can be even more affected by relativistic effects. It should be also noted that the H_2 ionization and dissociation energies are $T \approx 180\,000$ K and $T \approx 52\,000$ K, respectively. Therefore β_m of order of 10^{-4} points the limit of molecular hydrogen observation. It is far from the β_m values assumed in Figs. 2 and 3, hence that strong line asymmetries as presented in these figures will not be seen in H_2 spectra.

VI. CONCLUSIONS

Our derivation of the relativistic Voigt profile demonstrates that the formula of Gerbal and Prud'Homme, which is given in Ref. [14], is not valid. On the other hand, we have provided strong analytical elements to support the validity of our formulation: the convergence of the RVP to the relativistic Gaussian profile of Ref. [13], in the limit of a negligible homogeneous broadening, as well as the convergence to the classical Voigt profile, in the nonrelativistic case (namely, $\beta_m \to 0$). Furthermore, we demonstrated the normalization of the RVP, another important argument to confirm the correctness of our formulation. Our study shows that the relativistic deformation of the Voigt profile is rather small and its observation appears very challenging. Nevertheless, laboratory experiments have already demonstrated that the shape of molecular transitions can be measured with SNR exceeding 10^5 and further improvements are still possible [7]. Moreover, a recent experiment expressly designed to observe an absorption spectrum at the shot-noise limit [29] seems to provide a concrete possibility for observing the relativistic Voigt profile.

ACKNOWLEDGMENTS

P.A. is grateful to the Ph.D. Committee of the International Ph.D. Program in Novel Physics Methodologies for Environmental Research of the Second University of Naples for supporting the stage at the Nicolaus Copernicus University of Toruń. The research is a part of the program of the National Laboratory FAMO in Toruń, Poland. The research is partially supported by the Foundation for Polish Science TEAM Project cofinanced by the EU European Regional Development Fund, and is partially supported by the National Science Centre, Poland, Projects No. DEC-2013/09/N/ST4/00327 and No. DEC-2011/01/B/ST2/00491. P.W. is partially supported by 1772-F grant (Faculty of Physics, Astronomy and Informatics, Nicolaus Copernicus University (Poland) resources for development of young scientists).

APPENDIX A: NUMERICAL EVALUATION FOR WEAK RELATIVISTIC LIMIT (SMALL β_m)

Direct numerical evaluation of the integral from Eq. (9) for small β_m is very difficult, mainly because of huge value of the exponent power. In the simplest case, for β_m not smaller than 10^{-4}, this problem can be overcome by taking the factor e^{-2/β_m^2} before the integral and restricting the upper integration limit to $1+20\beta_m^2$. In other words the factor $\int_1^\infty d\gamma e^{-2\gamma/\beta_m^2}$ from Eq. (9) should be replaced with $e^{-2/\beta_m^2}\int_1^{1+20\beta_m^2} d\gamma e^{-2(\gamma-1)/\beta_m^2}$. However, for β_m smaller than 10^{-4} further modifications of Eq. (9) are needed. First, as it was done in Sec. III, the modified Bessel function of the second kind $K_2(2/\beta_m^2)$ should be replaced with $\sqrt{\pi}(\beta_m/2)\exp(-2/\beta_m^2)$. Moreover the integration variable γ should be substituted with $\beta_m^2\tilde{\gamma}+1$ and consequently the integration limits $\langle 1, 1+20\beta_m^2\rangle$ with $\langle 0, 20\rangle$. We also expand the $\beta_m \ln(\frac{1+\sqrt{1-\gamma^{-2}}}{1-\sqrt{1-\gamma^{-2}}})$ term with respect to β_m obtaining $\beta_m^2 2\sqrt{2}\tilde{\gamma}^{1/2}$. Finally Eq. (9) can be written in the following form:

$$I_{\mathrm{RVP}}(\Delta\omega) \approx \frac{2\sigma_0}{\pi^{3/2}}\frac{\Gamma'}{\beta_m^2\Gamma'^2+\omega_D^2}\int_0^{20} d\tilde{\gamma}e^{-2\tilde{\gamma}}\left(\beta_m^2\tilde{\gamma}+1\right) \times\left\{\frac{\omega_D}{\Gamma'}\left[\arctan\left(\tilde{\xi}_+(\tilde{\gamma})\right)-\arctan\left(\tilde{\xi}_-(\tilde{\gamma})\right)\right] +\beta_m^2 2\sqrt{2}\sqrt{\tilde{\gamma}}+\frac{1}{2}\beta_m\ln\left(\frac{1+\tilde{\xi}_-^2(\tilde{\gamma})}{1+\tilde{\xi}_+^2(\tilde{\gamma})}\right)\right\}, \quad \text{(A1)}$$

where

$$\tilde{\xi}_\pm(\tilde{\gamma}) \approx \left(\frac{\Delta\omega}{\Gamma'}\pm\frac{\omega_D}{\Gamma'}\sqrt{2}\tilde{\gamma}^{1/2}\right)+\beta_m\left(\frac{\omega_D}{\Gamma'}\tilde{\gamma}\pm\sqrt{2}\frac{\Delta\omega}{\Gamma'}\tilde{\gamma}^{1/2}\right) +\beta_m^2\left(\frac{\Delta\omega}{\Gamma'}\tilde{\gamma}\pm\frac{\sqrt{2}}{4}\frac{\omega_D}{\Gamma'}\tilde{\gamma}^{3/2}\right)\pm\beta_m^3\left(\frac{\sqrt{2}}{4}\frac{\Delta\omega}{\Gamma'}\tilde{\gamma}^{3/2}\right). \quad \text{(A2)}$$

Equation (A2) was obtained by expanding the expression from Eq. (10) with respect to β_m. The β_m^3 term in Eq. (A2) can be neglected for $\beta_m < 10^{-4}$.

APPENDIX B: RVP NORMALIZATION

In this Appendix we show analytically that, independently from all the parameters, the area of the RVP, given by Eq. (9), is equal to σ_0. This property, together with the limit cases checked in Secs. III and IV, is crucial to confirm the correctness of Eq. (9).

The integral from Eq. (9) over γ is not doable analytically. Hence, we first integrate this expression over $\Delta\omega$ from $-\infty$ to $+\infty$ and then over γ. It is convenient to introduce dimensionless variable $y = \Delta\omega/\omega_D$. In this section by integral $\int_{-\infty}^{+\infty}\ldots dy$ we mean the Cauchy principal value defined as $\lim_{y_0\to+\infty}\int_{-y_0}^{+y_0}\ldots dy$.

We first consider the term from Eq. (9) with arctan functions. After a few steps it can be shown that the integration over y leads to the simple formula

$$\int_{-\infty}^{+\infty} dy\left[\arctan\left(\xi_+(\gamma)\right)-\arctan\left(\xi_-(\gamma)\right)\right]=\frac{2\pi}{\beta_m}\sqrt{\gamma^2-1}. \quad \text{(B1)}$$

This allows to easily do the integral over γ from Eq. (9)

$$\int_1^{+\infty} d\gamma e^{-\frac{2\gamma}{\beta_m^2}}\gamma\frac{\omega_D^2}{\Gamma'}\int_{-\infty}^{+\infty} dy\left[\arctan\left(\xi_+(\gamma)\right)-\arctan\left(\xi_-(\gamma)\right)\right] =\pi\beta_m K_2\left(2/\beta_m^2\right)\times\frac{\omega_D^2}{\Gamma'}. \quad \text{(B2)}$$

It should be noted that the $\xi_{\pm}(\gamma)$ functions depend also on y, however to make the equations more readable we do not indicate it explicitly.

Similarly, several steps are needed to integrate the logarithmic terms from Eq. (9) over y

$$\int_{-\infty}^{+\infty} dy\left[\ln\left(\frac{1+\sqrt{1-\gamma^{-2}}}{1-\sqrt{1-\gamma^{-2}}}\right)+\frac{1}{2}\ln\left(\frac{1+\xi_{-}^{2}(\gamma)}{1+\xi_{+}^{2}(\gamma)}\right)\right] = 2\pi\frac{\Gamma'}{\omega_D}\sqrt{\gamma^2-1}. \tag{B3}$$

Then we do the integral over γ from Eq. (9)

$$\int_{1}^{+\infty} d\gamma e^{-\frac{2\gamma}{\beta_m^2}}\gamma\omega_D\beta_m\int_{-\infty}^{+\infty} dy\left[\ln\left(\frac{1+\sqrt{1-\gamma^{-2}}}{1-\sqrt{1-\gamma^{-2}}}\right)+\frac{1}{2}\ln\left(\frac{1+\xi_{-}^{2}(\gamma)}{1+\xi_{+}^{2}(\gamma)}\right)\right] = \pi\beta_m K_2\left(2/\beta_m^2\right)\times\beta_m^2\Gamma'. \tag{B4}$$

The sum of the right-hand sides of Eqs. (B2) and (B4) is

$$\pi\beta_m K_2\left(2/\beta_m^2\right)\times\left(\frac{\omega_D^2+\beta_m^2\Gamma'^2}{\Gamma'}\right), \tag{B5}$$

which cancels with the factor before the integral in Eq. (9) and hence

$$\int_{-\infty}^{+\infty} I_{\mathrm{RVP}}(\Delta\omega)d(\Delta\omega)=\sigma_0. \tag{B6}$$

It should be noted that only positive frequencies are physically meaningful, hence, in general, to obtain the line area the profile should be integrated only from $\omega=0$ to ∞ or correspondingly the integral over $\Delta\omega$ from Eq. (B6) should goes from $-\omega_D/\beta_m$ to ∞. On the other hand, it is seen in Fig. 3 that for nonzero Γ' the contribution to profile area comes also from negative ω (to the left of the gray vertical dashed line in Fig. 3). This means that the RVP, given by Eq. (9), is not normalized in the range from $\omega=0$ to ∞. It is caused by the fact that in our considerations we neglected the resonance around the $-\omega_0$ frequency or, in other words, we assumed rotating wave approximation [30]. Taking into account both $-\omega_0$ and $+\omega_0$ contributions we obtain normalized profile in the range from $\omega=0$ to ∞, see thin dashed lines in Fig. 3.

[1] S. A. Diddams, D. J. Jones, J. Ye, S. T. Cundiff, J. L. Hall, J. K. Ranka, R. S. Windeler, R. Holzwarth, Th. Udem, and T. W. Hänsch, Phys. Rev. Lett. **84**, 5102 (2000).

[2] S. Bartalini, P. Cancio, G. Giusfredi, D. Mazzotti, P. DeNatale, S. Borri, I. Galli, T. Leveque, and L. Gianfrani, Opt. Lett. **32**, 988 (2007).

[3] D. Gatti, A. Gambetta, A. Castrillo, G. Galzerano, P. Laporta, L. Gianfrani, and M. Marangoni, Opt. Express **19**, 17520 (2011).

[4] J. Domysławska, S. Wójtewicz, D. Lisak, A. Cygan, F. Ozimek, K. Stec, Cz. Radzewicz, R. S. Trawiński, and R. Ciuryło, J. Chem. Phys. **136**, 024201 (2012).

[5] G.-W. Truong, D. A. Long, A. Cygan, D. lisak, R. D. van Zee, and J. T. Hodges, J. Chem. Phys. **138**, 094201 (2013).

[6] P. Wcisło, A. Cygan, D. Lisak, and R. Ciuryło, Phys. Rev. A **88**, 012517 (2013).

[7] A. Cygan, D. Lisak, S. Wójtewicz, J. Domysławska, J. T. Hodges, R. S. Trawiński, and R. Ciuryło, Phys. Rev. A **85**, 022508 (2012).

[8] L. Moretti, A. Castrillo, E. Fasci, M. D. De Vizia, G. Casa, G. Galzerano, A. Merlone, P. Laporta, and L. Gianfrani, Phys. Rev. Lett. **111**, 060803 (2013).

[9] C. Lemarchand, S. Mejri, P. L. T. Sow, M. Triki, S. K. Tokunaga, S. Briaudeau, C. Chardonnet, B. Darquie, and C. Daussy, Metrologia **50**, 623 (2013).

[10] D. Dravins, Astron. Nachr. **331**, 535 (2010).

[11] R. M. Wagner, L. M. Edwards, O. Kuhn, D. Thompson, and C. Veillet, Proc. of SPIE **9147**, 914705 (2014).

[12] M. Steffen and K. G. Strassmeier, Astron. Nachr. **328**, 632 (2007).

[13] Y.-S. Huang, J.-H. Chiue, Y.-C. Huang, and T. C. Hsiung, Phys. Rev. A **82**, 010102(R) (2010).

[14] D. Gerbal and M. Prud'Homme, J. Quant. Spectrosc. Radiat. Transfer **14**, 351 (1974).

[15] P. Maddaloni, P. Malara, E. De Tommasi, M. De Rosa, I. Ricciardi, G. Gagliardi, F. Tamassia, G. Di Lonardo, and P. De Natale, J. Chem. Phys. **133**, 154317 (2010).

[16] G. D. Dickenson, M. L. Niu, E. J. Salumbides, J. Komasa, K. S. E. Eikema, K. Pachucki, and W. Ubachs, Phys. Rev. Lett. **110**, 193601 (2013).

[17] C.-F. Cheng, Y. R. Sun, H. Pan, J. Wang, A.-W. Liu, A. Campargue, and S.-M. Hu, Phys. Rev. A **85**, 024501 (2012).

[18] S. Kassi and A. Campargue, J. Mol. Spectrosc. **300**, 55 (2014).

[19] T. Tsuji, Ann. Rev. Astron. Astrophys. **24**, 89 (1986).

[20] K. H. Hinkle, B. Aringer, T. Lebzelter, C. L. Martin, and S. T. Ridgway, Astron. Astrophys. **363**, 1065 (2000).

[21] K. Menou and E. Rauscher, Astrophys. J. **713**, 1174 (2010).

[22] J. G. Ingalls, T. M. Bania, F. Boulanger, B. T. Draine, E. Falgarone, and P. Hily-Blant, Astrophys. J. **743**, 174 (2011).

[23] T. Tsuji, Astron. Astrophys. **122**, 314 (1983).

[24] O. Cardona, A. Flores, and L. H. Rodrígues-Merino, Astrophys. **54**, 538 (2011).

[25] R. Ciuryło, Phys. Rev. A **58**, 1029 (1998).

[26] A. Einstein, Ann. der Phys. **322**, 891 (1905).

[27] E. Eriksen and Ø. Grøn, Am. J. Phys. **55**, 363 (1987).

[28] F. Jüttner, Ann. Phys. (Berlin, Ger.) **339**, 856 (1911).

[29] G.-W. Truong, J. D. Anstie, E. F. May, T. M. Stace, and A. N. Luiten, Phys. Rev. A **86**, 030501(R) (2012).

[30] W. Demtröder, *Laser spectroscopy* (Springer, Berlin, 2003).